SPECIAL
Air-sea interaction during PISTON-MISOBOB-CAMP2Ex
COLLECTION

Fast Floating Temperature Sensor Measures SST, Not Wet-Bulb Temperature

SIMON P. DE SZOEKE[a]

[a] *College of Earth, Ocean, and Atmospheric Sciences, Oregon State University, Corvallis, Oregon*

(Manuscript received 25 November 2020, in final form 4 March 2021)

ABSTRACT: A small integrated oceanographic thermometer with a nominal response time of 1 s was affixed to a floating hose "sea snake" towed near the bow of a research vessel. The sensor measured the near-surface ocean temperature accurately and in agreement with other platforms. The effect of conduction and evaporation is modeled for a sensor impulsively alternated between water and air. Large thermal mass makes most sea snake thermometers insensitive to temperature impulses. The smaller 1-s thermometer cooled by evaporation, but the sensor never reached the wet-bulb temperature. The cooling was less than 6% of the (~2.7°C) difference between the ocean temperature and the wet-bulb temperature in 99% of 2-s^{-1} samples. Filtering outliers, such as with a median, effectively removes the evaporative cooling effect from 1- or 10-min average temperatures.

SIGNIFICANCE STATEMENT: Floating "sea snake" thermometers measure the near-surface ocean temperature accurately and robustly within 0.1 m of the surface, where solar warming affects the ocean temperature. These temperature measurements are used to verify satellite sea surface temperature retrievals and to track the exchange of heat and moisture between the ocean and atmosphere. Most sea snake thermometers are several hundred grams and respond slowly to ocean temperature. The slow response makes the thermometer less sensitive to air temperature, should it jump into the air due to waves or ship motion, and thus more representative of the ocean temperature. Observations from this study show that a sea snake sensor with a short 1-s response is also suitable for near-surface ocean temperature measurements.

KEYWORDS: In situ oceanic observations; Quality assurance/control; Ship observations

1. Introduction

The temperature profile of the upper meter of the ocean is sensitive to radiative absorption, turbulent surface heat flux, mixing by wind and convection, molecular viscosity, and wave effects. Solar absorption results in a diurnal warm layer near-surface temperature maximum below a molecular cool skin (e.g., Stuart-Menteth et al. 2005; Kawai and Wada 2007). Floating thermistors measure diurnal warm layers. Diurnal warm layers affect SST remote sensing, so measurements in situ are important for validating sea surface temperature (SST) retrievals (Emery et al. 2001; Donlon et al. 2002; Gentemann et al. 2003). Accurate SST measurements are also critical for modeling surface turbulent sensible and latent heat flux with bulk aerodynamic formulas (Fairall et al. 1996a,b). The warm layer has a strong effect on the bulk fluxes where differences between SST and air temperature are small.

Interactions between the ocean, atmosphere, and surrounding land in the Bay of Bengal can reverse the sign of the air–sea temperature difference and surface fluxes (Bhat and Fernando 2016), so the sign of the flux is sensitive to diurnal warming. The Monsoon Intraseasonal Oscillations in the Bay of Bengal (MISO-BOB) experiment measured processes in the ocean and atmosphere—diurnal warm layers, ocean fronts and stratification, atmospheric convection, and surface meteorology and fluxes—related to the evolution of SST and the monsoon. SST in the Bay of Bengal affects monsoon intraseasonal oscillations through resonant air–sea interactions (Sengupta et al. 2001; Zhang et al. 2018).

The finescale temperature structures in the upper meter of the ocean are easily disturbed or destroyed by the wakes of observing platforms such as ships, buoys, or sensor housings. Wind, waves, salt, and sun foul, corrode, and buffet sensors, making the upper meter of the ocean a challenging environment for sensors to endure and make good measurements. Robust platforms for measuring the upper meter of the ocean in situ include bow chains (Moulin et al. 2018), high-resolution towed profilers, and floating "snake" or "otter" platforms dragged abeam to avoid the ship's wake (e.g., Hughes et al. 2020).

The NOAA Physical Sciences Laboratory (PSL) sea snake sensor continuously measures near-surface ocean temperature at 0.1 m depth (Curry et al. 2004). The sea snake consists of a thermistor in an aerodynamic, floating, and strain-relieving plastic hose, dragged from forward of the beam of a ship, so that the thermistor floats at a consistent depth whether the ship is stationary, underway, or maneuvering. The temperature measured by the sea snake is representative of the ocean

Denotes content that is immediately available upon publication as open access.

Corresponding author: Simon P. de Szoeke, simon.deszoeke@oregonstate.edu

DOI: 10.1175/JTECH-D-20-0193.1

surface diurnal warm layer. The molecular cool skin is not resolved by the measurement, but can be modeled (Paulson and Simpson 1981; Fairall et al. 1996b).

When the ship moves at high speed relative to the sea, the water measured by the sea snake is affected by the ship wake. Waves lift and pull the sea snake and the sensor occasionally jumps out of the water into the near-surface air. In the cooler air, evaporation and conduction cool the sensor relative to the ocean. Despite the jumping, the sea snake measures a temperature representative of the near-surface ocean, because of the greater thermal conductivity of water compared to that of air, the small fraction of time spent in the air compared to in the water, and the long time constant of the (0.2 kg) thermally conductive sensor body.

A small commercially produced RBRsolo sensor was attached to the floating hose of the sea snake in leg 2 of the 2019 MISO-BOB field experiment. The RBRsolo integrates a calibrated thermistor circuit, data logging, and power. The RBRsolo is considerably smaller than the PSL sea snake.

The objective of this article is to model and to test the potential for commercial fast-response (1-s) oceanographic thermometers to measure near-surface ocean temperature. This is demonstrated with analysis of observations from a fast thermometer deployed in the Bay of Bengal, and with a model of how conduction and evaporation affect the thermometers. Section 2 introduces near-surface ocean temperature observations from the Bay of Bengal in 2019. Section 3 models the effect of sensor adjustment time on the temperature measured by a jumping sensor, demonstrating why even the small RBRsolo sensor is mostly representative of ocean temperature. Section 4 shows the RBRsolo temperature measurements are mostly representative of the near-surface ocean temperature, compared to wet-bulb temperature and other contemporaneous ocean temperature measurements. Section 5 summarizes that fast-response sensors can be used to estimate near surface ocean temperature, and recommends a 0.6th quantile filter to remove the occasional effect of air cooling.

2. Near-surface ocean temperature measurements in the Bay of Bengal

Several near-surface temperature measurements are available during the MISO-BOB 2019 experiment. The Scripps Institution of Oceanography Fast Current–Temperature–Depth (FCTD) measured ocean temperature with around-the-clock profiling for most of the cruise. The Oregon State University SurfOtter was deployed for intervals of several days. The SurfOtter sampled the upper 2 m of the ocean with an array of temperature probes similar to the one attached to the sea snake. SurfOtter provides independently calibrated ocean temperature measurements at 0.2 m depth that corroborate the FCTD and RBRsolo on the sea snake.

Ship thermosalinographs (TSGs) measure temperature at the intake depth of ~5 m. In MISO-BOB 2019 the ship's two TSGs suffered from a number of issues, including variable flow, air locking of the flow-through plumbing and pumps, and digital sensor spikes. As a result, the TSG temperature drifted with variable offsets from the other ocean temperature sensors.

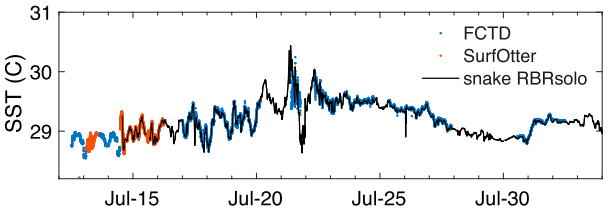

FIG. 1. Near-surface ocean temperature (SST) measured during the Monsoon Intraseasonal Oscillations in the Bay of Bengal (MISO-BOB) research cruise in 2019. Time series are interpolated to 1 min from the Scripps Fast CTD (FCTD) casts at 3 m depth (blue), 1-min means from the Oregon State University SurfOtter at 0.2 m (orange), and averaged to 1 min using the 0.6th quantile of RBRsolo attached to the NOAA PSL sea snake floating at 0.1 m (black).

The wire resistance of the PSL sea snake thermistor circuit drifted due to weathering of an extension cable.

Issues with the TSGs and sea snake motivated workers to attach an RBRsolo ocean temperature sensor to the floating hose of the sea snake. Tension on the sea snake hose and bow waves make the sea snake and the attached RBRsolo jump out of the water. Neglecting radiation, the sensor cools due to temperature conduction and evaporative heat loss. Despite these issues, the RBRsolo sensor continuously and reliably measured ocean temperature. Figure 1 shows ocean temperature for 12 July–2 August 2019, from the 10-min average of RBRsolo on the sea snake, FCTD cast temperature at the top of the profile (every 110 s), and the SurfOtter (every 0.5 s). The RBRsolo 10-min average is the mean of the 0.6 quantiles over each 1 min of 2-s^{-1} samples.

The sea snake RBRsolo mostly agrees with contemporaneous measurements from the FCTD and SurfOtter within ±0.01°C. The mean offset between the FCTD and RBRsolo drifts over several hours. Deployed astern of the ship, FCTD measurements at 3 m depth are often in the ship's wake, which could be responsible for the small and variable offset. The offset is nearly constant for the shorter deployments of the SurfOtter. Towed outboard of the ship's wake, the SurfOtter positions its sensor consistently at 0.2 m depth. The 2-s^{-1} SurfOtter temperature time series shows microstructure with variable amplitude about the mean of 0.01°–0.04°C. Brief temperature differences of ~0.5°C between the FCTD and sea snake RBRsolo are not explained (Fig. 1, e.g., at the start and end of the 21 July FCTD deployment, the start of the 22 July deployment, and at 0100 UTC 25 July).

3. Model of the effect of the floating sensor jumping out of the water

Here, a model for the conductive and evaporative effects on the thermometer demonstrates that a thermometer with slow response time is relatively insensitive to the effect of cooling due to jumping out of the water. Even the RBRsolo, with its relatively short response time, is not strongly affected by cooling due to jumping.

The effect of the jumps on the mean temperature measured by the sensor depends on the ratio of the duration of the jumps

to the response time of the sensor. If the jumps are much longer than the response time, the sensor comes to equilibrium with its surroundings during each jump and each immersion, so its average temperature is the weighted mean of the air temperature weighted by the fraction f of time spent in the air, and the ocean temperature weighted by $(1 - f)$. In this fast-response limit, the mean temperature measurement is sensitive to the jump fraction f, but the difference in the conductivities between air and water is unimportant. If the duration of the jumps are small compared to the time response of the sensor, as it is for a massive thermometer, then the mean temperature measured is less sensitive to the jumps due to the lower conductivity of air. The sensor temperature adjusts toward the air and ocean temperatures in proportion to their conductivities.

The sea snake measures a temperature representative of the water temperature because of the water's greater conductivity and because it spends most of the time in the water. The sea snake measures the temperature inside of a large (0.207 kg) cylindrical brass hose fitting, increasing its response time. The water and air conduct their temperature to the sea snake sensor body, and the thermal mass of the body integrates the temperature response to the outside temperature.

The mass of the RBRsolo thermistor housing is much smaller, with a smaller extensive heat capacity and shorter conductive time scale than the sea snake. RBR claims a time response of ~1 s for the RBRsolo in water. The RBRsolo samples at $2\,s^{-1}$, faster than its time constant. The instantaneous samples reflect the instantaneous temperature of the thermistor, which may be equilibrated with the ocean or air, or adjusting to jumping out or to reentering the water.

a. Response to a single impulse

When jumping from the water into the air, or vice versa, the sensor temperature adjusts to the impulsive change to the new temperature of the surroundings $T(\infty)$. When the sensor experiences the temperature impulse $\delta = T(\infty) - T(0)$ at time $t = 0$ its temperature adjusts with time scale τ as

$$T(t) = T(0) + \delta[1 - \exp(-t/\tau)].$$

The adjustment-scaled relative temperature anomaly

$$\phi(r) = [T(r) - T(0)]/\delta = 1 - \exp(-r)$$

adjusts from $\phi = 0$ asymptotically toward $\phi = 1$ as function of the scaled adjustment time $r = t/\tau$. Figure 2 shows the normalized final temperature $\phi(r)$ (blue) and mean temperature (red)

$$\overline{\phi}(r) = 1 + [\exp(-r) - 1]/r$$

over the adjustment interval $[0, r]$.

b. Temperature sensor time constants

1) CONDUCTION

The response of the sensor depends on the thermal conductivity. The time response in water for the RBRsolo is specified by the manufacturer as $\tau_{oc} = 1$ s. The thermal conductivity of seawater ($0.594\,W\,m^{-1}\,K^{-1}$) is 24 times greater than that of air ($0.026\,W\,m^{-1}\,K^{-1}$), so the conductive time scale in air is estimated as $\tau_{cond} = 24$ s.

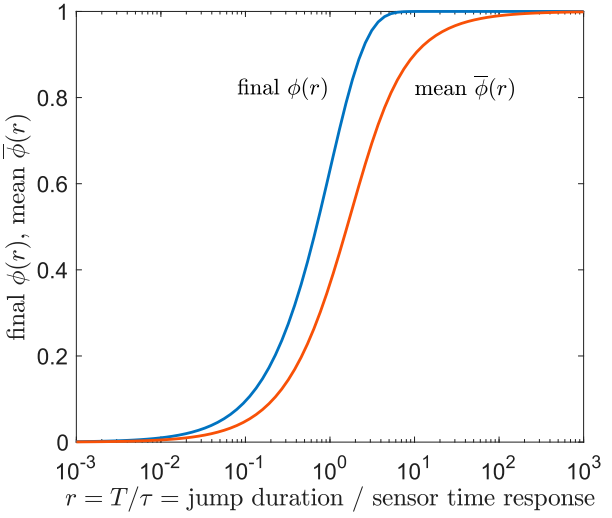

FIG. 2. Temperature response $\phi(r)$ at scaled time r (blue) and averaged from $[0, r]$ (red) of a sensor with time response τ to an impulsively changed temperature at time 0.

2) EVAPORATIVE EFFECTS

The sensor remains wet when it jumps. Water evaporates from the sensor, cooling it toward the wet-bulb temperature T_w, at which evaporative cooling balances thermal conduction from the air. This evaporation into the air is governed by water vapor diffusion. The sensor temperature changes from the sum of evaporative and diffusive heat fluxes,

$$\frac{dT}{dt} = -\frac{A}{M}\frac{\rho_{air}}{l}\left[\frac{L}{c_p}K_q\left(\frac{dq_s}{dT}\right)_{T_w} + K_T\right](T - T_w),$$

where A/M are extensive constants that depend on the mass and surface area of the sensor. The effective thickness of the laminar diffusive layer is l, $K_q = 8.8 \times 10^{-5}\,m^2\,s^{-1}$ is the kinematic molecular diffusivity of water vapor in air, and $K_T = D_T/(\rho_{air}c_p) = 2.25 \times 10^{-5}\,m^2\,s^{-1}$ is the kinematic molecular conductivity of temperature in air. Including the evaporative heat loss coefficient, the term in square brackets is $\beta = 13.8$ times greater than the heat conductivity K_T alone. The evaporative–conductive time constant for a wet sensor is $\tau_{air} = \tau_{cond}/\beta$. Including evaporation, the cooling time scale in air $\tau_{air}/\tau_{oc} = (24/13.8) = 1.74$ (Table 1). Thus, the time constant for a wet sensor in air is nearly twice as long as for the sensor immersed in water.

Average wet-bulb temperature T_w of the air is cooler than near-surface ocean temperature by 2.7°C during MISO-BOB 2019. The ocean skin temperature is cooler than the temperature measured by the floating thermistor and warmer than the wet-bulb temperature, because it is cooled by evaporation and warmed by conduction from the ocean water below.

c. Response to a succession of regular jump cycles

The timing of the sensor's jumps is actually intermittent and unpredictable. The simplified model here estimates an equilibrium temperature resulting from a succession of regular

TABLE 1. Estimated sensor conductive response times τ in water and air for the RBRsolo, jump duration times T, and scaled adjustment times $r = T/\tau$.

	τ (s)	T (s)	r
Ocean conduction	1	5	5
Air conduction alone	24	0.5	0.02
Air conduction and evaporation	1.74	0.5	0.29

identical jump cycles with period P and duty cycle, or fraction of time in the air, f. Adjusting alternately to the water and the air, the sensor temperature is piecewise continuous, with scaled times $r_{oc} = (1 - f)P/\tau_{oc}$ and $r_{air} = fP/\tau_{air}$ and adjustment times from section 3b (Table 1).

The absolute scaled temperature is

$$\theta = (T - T_{oc})/(T_w - T_{oc}),$$

so that $\theta = 0$ is the scaled ocean temperature and $\theta = 1$ is the scaled air wet-bulb temperature. At equilibrium, the temperature returns to the same value in each cycle. Solving using this condition, the temperature of the sensor at the end of the adjustment to the air just before returning to the ocean is

$$\theta_{air}(r_{air}) = \frac{1 - \exp(-r_{air})}{1 - \exp(-r_{air} - r_{oc})}.$$

The temperature of the sensor in the ocean just before the next jump into the air is

$$\theta_{oc}(r_{oc}) = \theta_{air}(r_{air})\exp(-r_{oc}).$$

The mean temperatures over the intervals in the air and the ocean are, respectively,

$$\overline{\theta}_{air} = 1 - \frac{(1 - \theta_{oc})[1 - \exp(-r_{air})]}{r_{air}},$$

$$\overline{\theta}_{oc} = \frac{\theta_{air}[1 - \exp(-r_{oc})]}{r_{oc}}.$$

The mean temperature for a whole cycle is their weighted sum, $\overline{\theta} = f\overline{\theta}_{air} + (1 - f)\overline{\theta}_{oc}$.

Figure 3 shows average scaled temperature $\overline{\theta}$ for various choices of jump period P and fraction (duty cycle) of the time jumping in air f. The contours of $\overline{\theta}$ inflect at $r_{air} = fP/\tau_{air} \approx 1$ (dashed line). For long jumps, $r_{air} \gg 1$, the temperature fully equilibrates with the air, so the scaled mean temperature approaches the duty cycle $\overline{\theta} = f$ (Fig. 3, right). For short jumps with $r_{air} \ll 1$ (Fig. 3, left), the mean scaled temperature is less than the duty cycle $\overline{\theta} = f(\tau_{oc}/\tau_{air})$, by the ratio of the adjustment time scales in air and water.

If the RBRsolo ($\tau_{oc} = 1$ s) jumps out of the water with a period of $P = 10$ s and a duty cycle $f = 0.05$, the mean scaled temperature is $\overline{\theta} = 0.033$. That is, the mean measured temperature would be lower than the near-surface ocean temperature by about 3.3% of the ocean–air temperature difference. If $T_w - T_{oc} = 2.7$°C then the mean temperature change due to the jumps is −0.09°C. This effect on the mean is near the temperature measurement accuracy required for bulk flux calculations.

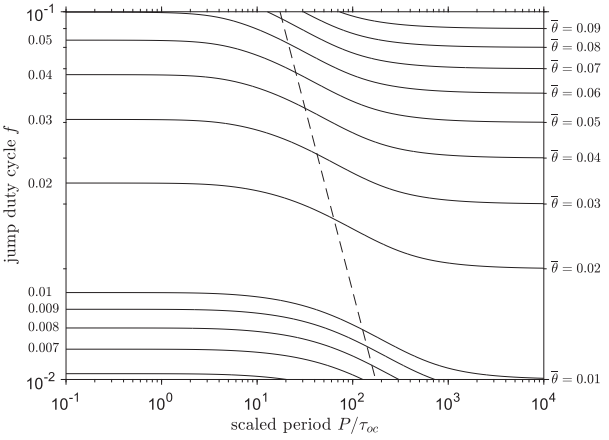

FIG. 3. Contours of mean scaled temperature $\overline{\theta}$ as a function of the fraction of time the sensor jumps out of the water and the period P/τ_{oc} scaled by the adjustment time scale of the sensor in water. The dashed line shows $r_{air} = fP/\tau_{air} = 1$

The large (0.207 kg) housing of the PSL sea snake thermistor integrates away quick temperature variations, making it less sensitive to temperature shocks by design. The mass and surface area of the cylindrical thermistor housing of the RBRsolo are estimated at 1.2 g and 310 mm^2, and the surface area of the PSL sea snake to be 6300 mm^2. The ratio of the time constants is then $\tau_{snake}/\tau_{solo} = (M_{snake}/M_{solo})(A_{snake}/A_{solo}) = 9$. The effect of the longer response time of the sea snake sensor is to increase the denominator in the x axis in Fig. 3, and thus to shift nearly one order of magnitude to the left. The longer response time improves the stability of the mean temperature, but only modestly. Shifting left near the transition at $r_{air} = 1$ (dashed line), the snake has a lower mean scaled temperature response to the jumps than the RBRsolo by about $\overline{\theta}_{snake} \approx (\tau_{oc}/\tau_{air})^{0.5}\overline{\theta}_{solo} \approx 0.8\overline{\theta}_{solo}$.

4. Results of measurements

The effect of cooling of the sensor jumping in air is small but measurable at the sampling frequency of 2 s^{-1}. The instantaneous RBRsolo temperature samples T_{solo} have strong outliers (Fig. 4). Most of the outliers are single isolated samples that stand 0.1°–1°C colder than the mode T_{solo}.

Despite infrequent outliers of T_{solo} approaching but not reaching the wet-bulb temperature, the distribution of T_{solo} has a strongly peaked mode at the near-surface ocean temperature T_{oc}, which agrees with the SurfOtter and FCTD near-surface ocean temperature. The outliers do not strongly affect the mean temperature. The 1-min mean temperature is only 7×10^{-3} °C lower than the 1-min mode on average. However, 1% of 1-min averages are at least 0.1°C cooler than the mode. To filter outliers from Fig. 1, the RBRsolo temperature in Fig. 1 is the 0.6th quantile of all 2-s^{-1} samples during each 1-min interval.

The quantiles of the T_{solo} measurements yield a simple method for filtering the outliers. Table 2 compares the median

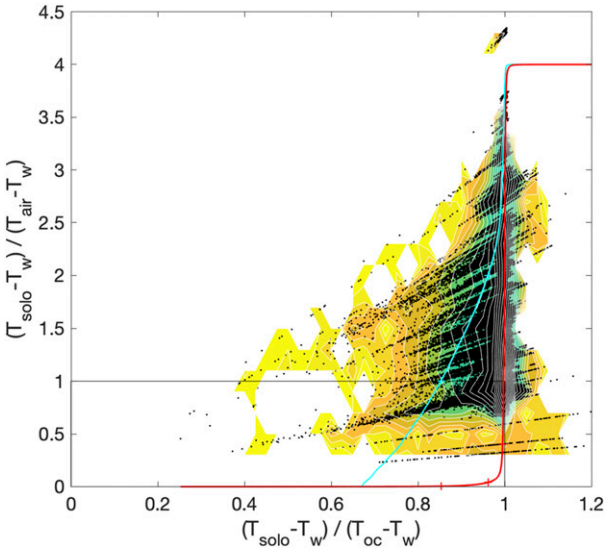

FIG. 4. Distribution of RBRsolo temperature in MISO-BOB leg 2, normalized by the difference between (air) wet-bulb temperature, and ocean (x axis) and air (y axis) temperature, respectively. White-filled contours represent doublings of frequency density. The red line is the cumulative distribution of $(T_{\rm solo} - T_w)/(T_{\rm oc} - T_w)$ (between 0 and 4 on the y axis), and cyan line is the logarithm of the cumulative distribution so that each unit on the y axis represents a decade (0.01th, 0.1th, 1st, 10th, 100th percentiles).

and root-mean-square of the difference between the 1-min 0.3th, 0.5th (i.e., the median), 0.6th, and 0.9th quantiles and the mode of $T_{\rm solo}$. The bias indicated by the median difference is small for all the quantiles, and smallest (4×10^{-5} °C) for the 0.6th quantile. The root mean squared difference is also smallest for the 0.6th quantile. Thus the 0.6th quantile is used to estimate $T_{\rm oc}$. The distribution of instantaneous $T_{\rm solo}$ relative to $T_{\rm oc}$ and T_w further justifies the $T_{\rm oc}$ estimate.

The two equilibrium temperatures to which $T_{\rm solo}$ adjusts are the near-surface ocean temperature $T_{\rm oc}$ and the wet-bulb temperature T_w. Figure 4 shows the distribution of temperature samples

$$(T_{\rm solo} - T_w)/(T_{\rm oc} - T_w) = 1 - \theta,$$

normalized by the ocean–wet-bulb temperature difference. (Note θ in section 3 is defined relative to $T_{\rm oc}$ rather than to T_w.) Temperature $T_{\rm solo}$ as cold as the wet-bulb temperature $[(T_{\rm solo} - T_w)/(T_{\rm oc} - T_w) = 0]$ was never observed. The record mean $\overline{(T_{\rm solo} - T_{\rm oc})/(T_w - T_{\rm oc})}$ is 0.998 yet its 1st percentile is 0.96, representing cooling of 4% of the temperature difference $T_{\rm oc} - T_w$. The y axis $(T_{\rm solo} - T_w)/(T_{\rm air} - T_w)$ of Fig. 4 shows the temperature relative to the interval between $T_{\rm air}$ and T_w. The horizontal line $(T_{\rm solo} - T_w)/(T_{\rm air} - T_w) = 1$ represents $T_{\rm solo} = T_{\rm air}$. Thirty percent of $T_{\rm solo}$ measurements are cooler than $T_{\rm air}$ and warmer than T_w. This significant fraction is because MISO-BOB had a number of days with stable surface layers ($T_{\rm air} > T_{\rm oc}$) and downward net turbulent heat fluxes (not shown).

5. Summary

Fast (1-s response) thermometer measurements in the upper meter of the ocean can be used to estimate near-surface ocean temperature accurately. Long term means are barely influenced by air cooling of the small RBRsolo sensor when it quickly jumps from the water. Shorter means of 1–10 min resolve oceanic variability on submesoscale and diurnal time scales, but simple 1- and 10-min means are in some cases affected by air cooling: 1% of 1-min means have air cooling greater than 0.1°C.

The model shows that the larger mass of the 0.2 kg sea snake does not simply linearly average temperature impulses. The effect of impulses is also minimized by slower adjustment of the thermometer to the air. The mean temperature from the fast-response thermometer is more sensitive to evaporative cooling impulses. While a larger thermometer barely changes from the ocean temperature, the fast-response thermometer more quickly approaches the wet-bulb temperature. The standard 0.2 kg sea snake sensor used by PSL has about an order of magnitude slower time response, making its mean temperature moderately less sensitive (−20%) to air cooling than the RBRsolo.

Outliers representative of cooling when the sensor briefly jumps into the air can be filtered. Filtering 2-s^{-1} samples with a quantile (e.g., median) filter effectively removes the air cooling effect from the RBRsolo temperature. A wide range of quantiles are representative of near-surface ocean temperature. The 0.6th quantile of the 2-s^{-1} samples within 1 min agrees with the mode. Employing suitable filtering, a fast sensor effectively estimates near-surface ocean temperature, despite cooling when the sensor jumps out of the water.

Estimates of surface evaporation depend on air surface humidity measurements. If some instantaneous samples from a fast thermistor attached to a jumping sea snake were representative of the wet-bulb temperature of the air, then these could be used for estimating air surface humidity. Though the faster temperature sensor adjusts more quickly than the 0.2 kg sea snake, its temperature is still representative of ocean temperature.

TABLE 2. Median difference between the 1-min 0.3th, 0.5th, 0.6th, and 0.9th quantiles of $T_{\rm solo}$ and its mode. Root-mean-square (rms) difference of the quantiles and the mode.

Quantile	0.3th	0.5th	0.6th	0.9th
Median quantile − mode (°C)	-5×10^{-3}	-1×10^{-3}	4×10^{-5}	6×10^{-3}
rms quantile (°C)	0.02	0.01	0.008	0.01

Acknowledgments. The author thanks S. Pezoa (NOAA PSL) for construction of and consultation on the sea snake floating thermometer, D. Lucas (Scripps Institution of Oceanography) for the near-surface FCTD measurements, E. Shroyer (OSU) for the SurfOtter measurements, and L. Johnson for insights on the manuscript. Meteorology data are available at the NOAA PSL FTP site: ftp://ftp1.esrl.noaa.gov/psd3/cruises/MISOBOB_2019/Sally_Ride/flux/Processed/. The near-surface ocean temperature data are available under the digital object identifier https://doi.org/10.7267/5138jn655 at Oregon State University Scholars Archives: https://ir.library.oregonstate.edu/concern/datasets/5138jn655. This work was supported by Office of Naval Research Award N00014-16-1-3094.

REFERENCES

Bhat, G. S., and H. Fernando, 2016: Remotely driven anomalous sea-air heat flux over the north Indian Ocean during the summer monsoon season. *Oceanography*, **29** (2), 232–241, https://doi.org/10.5670/oceanog.2016.55.

Curry, J. A., and Coauthors, 2004: SEAFLUX. *Bull. Amer. Meteor. Soc.*, **85**, 409–424, https://doi.org/10.1175/BAMS-85-3-409.

Donlon, C. J., P. J. Minnett, C. Gentemann, T. J. Nightingale, I. J. Barton, B. Ward, and M. J. Murray, 2002: Toward improved validation of satellite sea surface skin temperature measurements for climate research. *J. Climate*, **15**, 353–369, https://doi.org/10.1175/1520-0442(2002)015<0353:TIVOSS>2.0.CO;2.

Emery, W. J., D. J. Baldwin, P. Schlüssel, and R. W. Reynolds, 2001: Accuracy of in situ sea surface temperatures used to calibrate infrared satellite measurements. *J. Geophys. Res.*, **106**, 2387–2405, https://doi.org/10.1029/2000JC000246.

Fairall, C. W., E. F. Bradley, J. S. Godfrey, G. A. Wick, J. B. Edson, and G. S. Young, 1996a: Cool-skin and warm-layer effects on sea surface temperature. *J. Geophys. Res.*, **101**, 1295–1308, https://doi.org/10.1029/95JC03190.

——, ——, D. P. Rogers, J. B. Edson, and G. S. Young, 1996b: Bulk parameterization of air-sea fluxes for Tropical Ocean-Global Atmosphere Coupled-Ocean Atmosphere Response Experiment. *J. Geophys. Res.*, **101**, 3747–3764, https://doi.org/10.1029/95JC03205.

Gentemann, C. L., C. J. Donlon, A. Stuart-Menteth, and F. J. Wentz, 2003: Diurnal signals in satellite sea surface temperature measurements. *Geophys. Res. Lett.*, **30**, 1140, https://doi.org/10.1029/2002GL016291.

Hughes, K. G., J. N. Moum, and E. L. Shroyer, 2020: Heat transport through diurnal warm layers. *J. Phys. Oceanogr.*, **50**, 2885–2905, https://doi.org/10.1175/JPO-D-20-0079.1.

Kawai, Y., and A. Wada, 2007: Diurnal sea surface temperature variation and its impact on the atmosphere and ocean: A review. *J. Oceanogr.*, **63**, 721–744, https://doi.org/10.1007/s10872-007-0063-0.

Moulin, A. J., J. N. Moum, and E. L. Shroyer, 2018: Evolution of turbulence in the diurnal warm layer. *J. Phys. Oceanogr.*, **48**, 383–396, https://doi.org/10.1175/JPO-D-17-0170.1.

Paulson, C. A., and J. J. Simpson, 1981: The temperature difference across the cool skin of the ocean. *J. Geophys. Res.*, **86**, 11 044–11 054, https://doi.org/10.1029/JC086iC11p11044.

Sengupta, D., B. N. Goswami, and R. Senan, 2001: Coherent intraseasonal oscillations of ocean and atmosphere during the Asian summer monsoon. *Geophys. Res. Lett.*, **28**, 4127–4130, https://doi.org/10.1029/2001GL013587.

Stuart-Menteth, A. C., I. S. Robinson, and C. J. Donlon, 2005: Sensitivity of the diurnal warm layer to meteorological fluctuations. Part II: A new parameterisation for diurnal warming. *J. Atmos. Ocean Sci.*, **10**, 209–234, https://doi.org/10.1080/17417530500529539.

Zhang, L., W. Han, Y. Li, and E. D. Maloney, 2018: Role of north Indian Ocean air–sea interaction in summer monsoon intraseasonal oscillation. *J. Climate*, **31**, 7885–7908, https://doi.org/10.1175/JCLI-D-17-0691.1.